Beaming Light from a Subwavelength Aperture

H. J. Lezec, *et al.*

Science **297**, 820 (2002);
DOI: 10.1126/science.1071895

Science (print ISSN 0036-8075; online ISSN 1095-9203) is published weekly, except the last week in December, by the American Association for the Advancement of Science, 1200 New York Avenue NW, Washington, DC 20005.

Beaming Light from a Subwavelength Aperture

H. J. Lezec,[1] A. Degiron,[1] E. Devaux,[1] R. A. Linke,[2] L. Martin-Moreno,[3] F. J. Garcia-Vidal,[4] T. W. Ebbesen[1*]

Light usually diffracts in all directions when it emerges from a subwavelength aperture, which puts a lower limit on the size of features that can be used in photonics. This limitation can be overcome by creating a periodic texture on the exit side of a single aperture in a metal film. The transmitted light emerges from the aperture as a beam with a small angular divergence (approximately ±3°) whose directionality can be controlled. This finding is especially surprising, considering that the radiating region is mainly confined to an area with lateral dimensions comparable to the wavelength of the light. The device occupies no more than one cubic micrometer and, when combined with enhanced transmission, suggests that a wide range of photonic applications is possible.

Light transmission through an individual aperture, such as a hole in an opaque screen, has been studied for centuries. According to standard diffraction theory, apertures much smaller than the wavelength of light transmit very poorly and diffract light in all directions uniformly. These two properties, transmission and diffraction, are considered fundamental constraints in manipulating light on a very small scale for technological purposes. Ideally, one would like to be able to not only get more light through such structures but also to channel it in a well-defined direction as a collimated beam. Here we demonstrate an approach to satisfy both requirements.

The excitation of surface waves, or surface plasmons, on metallic surfaces give us a path to achieving this goal. Surface plasmons (SPs) are collective electronic excitations, or charge density waves, which are characterized by intense electromagnetic fields confined to the surface (*1–4*). For instance, SPs can boost the transmission of light through subwavelength hole arrays in metal films (*5–7*), a phenomenon which has been analyzed theoretically by various groups (*8–15*).

One way to couple free propagating light to surface plasmons is to have a periodic structure on the surface to satisfy conservation of energy and momentum. Therefore, a single aperture surrounded by a periodic corrugation in the metal surface will also display surface plasmon–enhanced transmission (*7*). Given that the coupling of light into SP modes is governed by geometrical momentum selection rules (i.e., occurs only at a specific angle for a given wavelength), we reasoned that the light exiting a single aperture might follow the reverse process in the presence of the periodic structure on the exit surface (*16–18*). In other words, the light might emerge preferentially at certain angles for certain wavelengths even in the case of a subwavelength aperture.

Structures designed to test this were fabricated by focused ion beam (FIB) milling of 300-nm-thick Ag films (FEI DB235 system using Ga^+ ions and a 5-nm nominal beam diameter). Free-standing suspended films were used to allow patterning of both input and exit sides independently (Figs. 1A and 2A). The transmission properties were measured with the use of an optical microscope and spectrometer. The light incident on the sample was collimated and kept at normal incidence while the transmitted light was collected at various angles.

For reference, we first analyzed the spectral and geometrical transmission properties of a single cylindrical hole (diameter d = 300 nm). At wavelengths $\lambda > 2d$, the exiting light is fully diffracted into a half-sphere, as expected. By patterning the input side around the hole with a concentric periodic groove structure (bull's eye), the transmission is boosted at wavelengths determined by the periodic corrugation due to coupling to SPs (*2–6*), but the light remains fully diffracted as in the case of the bare hole. The resulting transmission boost in the present case is on the order of a factor of 10.

We then patterned an identical bull's eye grating of the same period around the exit side of the hole. For illumination at normal incidence, a strong transmission peak is evident around 660 nm, a wavelength slightly larger than the 600-nm period of the grooves (Fig. 1B). By recording the transmission spectra at various angles on the exit side (using a collection aperture with an angular resolution of ±3°), a strong dependence is observed (Fig. 1B). A plot of the transmission intensity as a function of angle (Fig. 1D) implies that the transmitted light

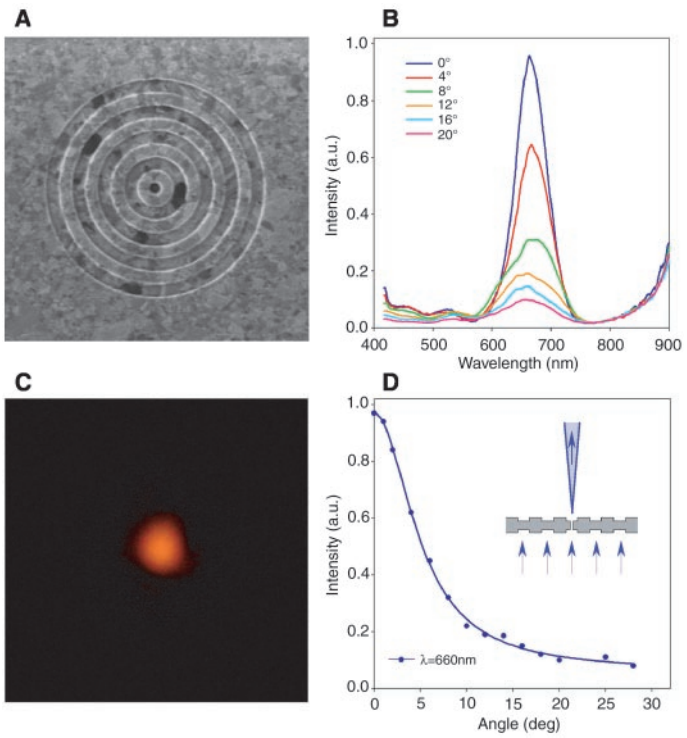

Fig. 1. (**A**) FIB micrograph image of a bull's eye structure surrounding a cylindrical hole in a suspended Ag film (groove periodicity, 500 nm; groove depth, 60 nm; hole diameter, 250 nm; film thickness, 300 nm). (**B**) Transmission spectra recorded at various collection angles for a bull's eye structure on both sides of a suspended Ag film (groove periodicity, 600 nm; groove depth, 60 nm; hole diameter, 300nm; film thickness, 300 nm). The tail above 800 nm is an artifact of the spectral measurement. The structure is illuminated at normal incidence with unpolarized collimated light. The spectra were measured using a Nikon TE200 microscope coupled to an Acton monochromator and a Princeton Instruments CCD (charge-coupled device) camera. (**C**) Optical image of the sample of (A) illuminated from the back at its wavelength of peak transmission (λ_{max} = 660 nm) using a 50-nm band-pass filter. (**D**) Angular transmission-intensity distribution derived from the spectra of (B) at λ_{max}. (Inset) Schematic diagram of the structure and the beam divergence and directionality of the transmitted light at λ_{max} in the far field.

[1]ISIS, Louis Pasteur University, 4 rue B. Pascal, 67000 Strasbourg, France. [2]NEC Research Institute, 4 Independence Way, Princeton, NJ 08540, USA. [3]Departamento de Fisica de la Materia Condensada, ICMA-CSIC, Universidad de Zaragoza, 50015 Zaragoza, Spain. [4]Departamento de Fisica Teorica de la Materia Condensada, Universidad Autonoma de Madrid, 28049 Madrid, Spain.

*To whom correspondence should be addressed. E-mail: ebbesen@isis-ulp.org

emerges in the shape of a well-defined beam with an observed a full-width at half-maximum (FWHM) divergence of ±5°. When the finite angular resolution of our apparatus is taken into account, the actual beam divergence is deduced to be ~±3°. This low divergence is all the more surprising, considering the small size of the apparent spot at the exit surface. Figure 1C shows an optical image of the exit surface of a bull's eye structure at its peak transmission wavelength, recorded at the same scale as the FIB image (Fig. 1A). Light emission is mainly confined to a central area around the hole with lateral dimensions not exceeding 1 μm or two periods of the structure.

To elucidate the physics of the beam formation on the exit side, we prepared and analyzed other structures. In particular, we studied a more basic structure with one dimensional symmetry consisting of a single slit surrounded by a linear groove array on both side of the film (Fig. 2A). The slit is 40 nm wide, 4400 nm long, and the corrugation has a 500-nm period.

By varying the output collection angle (Fig. 2B), we determined that the transmission spectrum is, again, angle-dependent. The maximum transmission intensity drops and the peak splits into two peaks that move to lower and higher wavelengths, respectively, implying that at a given wavelength the light emerges with maximum intensity at a particular angle from the surface. For example at $\lambda = 580$ and 800 nm, the corresponding values are 0° and 30° from the normal, respectively. As in the case of the bull's eye structure of Fig. 1, the measured FWHM divergence of these lobes is ±5° (Fig. 2D), which corresponds to an actual divergence of ±3° when corrected for our angular resolution. In the absence of corrugation on the output surface, the narrow slit diffracts the transmitted light isotropically.

To verify the equivalence of the in- and out-coupling mechanism between light and the metallic corrugated surface, we compared the dispersion relation governing the respective processes. The beam output angle as a function of wavelength matches quite well the input dispersion relation for such a grating (inset, Fig. 2B). This strongly indicates that SP modes are involved in a similar manner on both the input and output sides. In other words, the activated surface modes reradiate back into propagating light, following the energy and momentum conservation dictated by the corrugated surface.

Once again the emission spot size, as measured with an optical microscope, is centered on the subwavelength aperture and is mainly confined to an area with lateral dimensions on the order of two periods (compare Fig. 2, A and C). To further demonstrate the confined spatial extent of the reradiating area, we recorded high-resolution images for numerous samples using an optical microscope and a near-field scanning optical microscope (NSOM). These images were then profiled (inset, Fig. 3) for a bull's eye structure at its wavelength of maximum transmission. The NSOM data was recorded at 1.5 μm above the structure with an uncoated tip in order to avoid evanescent coupling with the surface plasmons. The FWHM are all ≤ 1 μm and, thus, are comparable to the optical wavelength.

The combination of low divergence angle and small emission area for the transmitted light is, at first glance, rather surprising. If we were to treat our structures as simple apertures, a standard far-field diffraction (*19*) calculation for $\lambda = 580$ nm (for instance, the peak wavelength in Fig. 2B) would require an aperture width of 4900 nm to achieve the observed divergence of ±3° FWHM, a width far larger than that of the

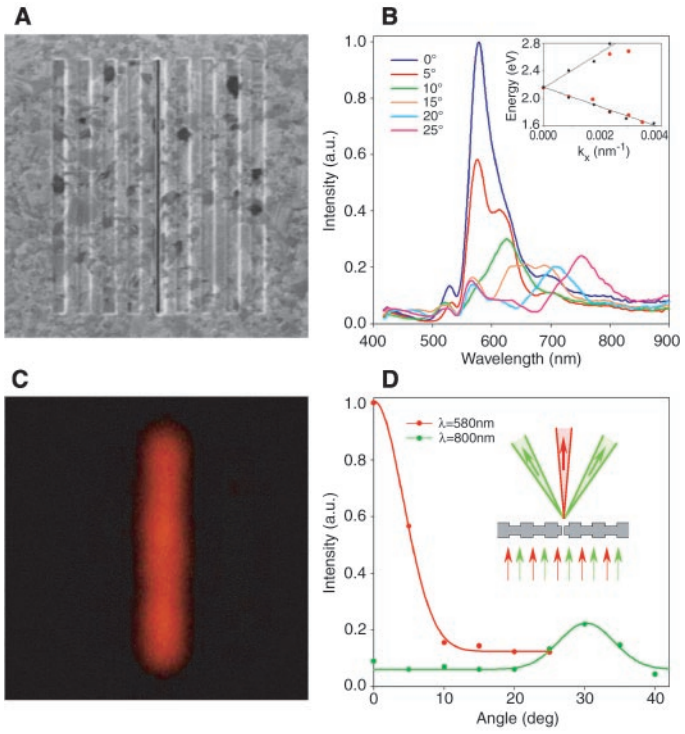

Fig. 2. (**A**) FIB micrograph image of a slit aperture with parallel grooves on both sides of a suspended Ag film (slit width, 40 nm; slit length, 4400 nm; groove periodicity, 500 nm; groove depth, 60 nm; film thickness, 300 nm). (**B**) Transmission spectra of the structure of (A) recorded at various collection angles. Illumination at normal incidence with light polarized perpendicular to the slit-length direction. The spectra were measured as in Fig. 1B. (Inset) Dispersion curve (black dots) of the periodic structure as well as the position of the spectral peaks (red dots), plotted as a function of collection angle. (**C**) Optical image of the sample of (A) illuminated from the back at its wavelength of peak transmission in the forward direction ($\lambda_{max} = 580$ nm) using a 50-nm band-pass filter. (**D**) Angular transmission-intensity distribution derived from the spectra of (B) at two selected wavelengths. (Inset) Schematic diagram of the structure showing the corresponding dependence of the directionality on wavelength and the beam divergence in the far field.

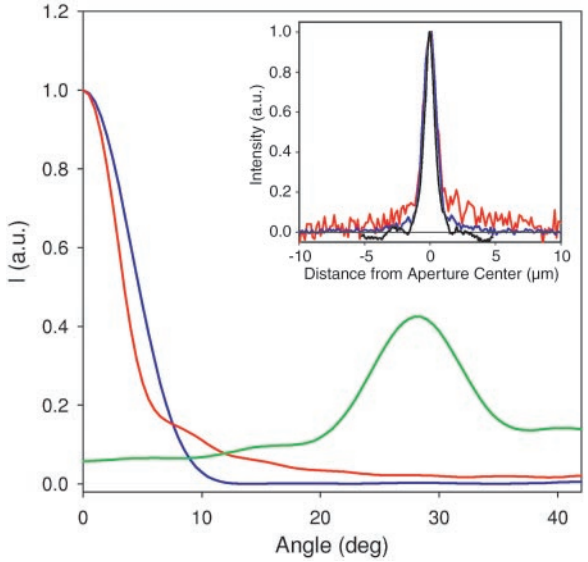

Fig. 3. Calculated far-field angular transmission intensity pattern of hole and slit structures of Figs. 1B and 2B. The wavelength conditions and legend color scheme are the same as in Figs. 1D and 2D. The calculation takes into account the finite acceptance angle of our equipment (± 3°). (Inset) Profile of the light intensity emitted as a function of distance from central aperture of bull's eye structure of Fig. 1B (blue curve) as compared to that of a bare hole (red curve) of same diameter (660-nm illumination wavelength). Black curve, NSOM profile in the case of a bull's eye pattern (period, 460 nm; aperture diameter, 230 nm; glass substrate) recorded at a height of 1.5 μm above the surface. For the NSOM measurement, the sample is illuminated on one side by a collimated beam (white light). The transmitted light is collected on the other side with a sharpened, uncoated optical fiber. Constant-height images are recorded using the procedure of (*4*).

actual openings in our experiments. This implies that the exit surface surrounding the aperture must also be involved in the reradiation process, as we already inferred from the existence of the dispersion relation. Nonetheless, we do not have uniform emission from an area as large as implied by the above estimate. If the structure surrounding the central aperture emitted light very weakly, could this contribute to explain the small observed angular divergence? Within the resolution limit of our apparatus, we cannot preclude the presence of some emission from the surface whose intensity diminishes rapidly as a function of lateral distance from the aperture. Given our optically thick film, the source of this emission can only come from scattering of the light emerging from the aperture. To test this possibility, we implemented a simple first-principle model based on interference in the far-field of light scattered at the center of each groove with a laterally variable emission intensity given by a curve fit to the experimental results (Fig. 3, inset). In our model, the phase of the emission at each groove is proportional to the distance travelled by the surface wave from its origin at the aperture. These SPs travel slightly slower than light in free space due to retardation by the metal and, as a consequence, emission normal to the surface occurs at a wavelength slightly larger than the period. With this model, we are able to reproduce the overall features of the observed angular divergence of Figs. 1D and 2D, as well as the dependence of directionality on wavelength (Fig. 3).

Perhaps the most non-intuitive aspect of this phenomenon is the fact that scattering at the grooves of only a small fraction of the light emerging from the aperture can create such a narrow beam by interference (*20*). Even though the emission remains heavily confined to the immediate vicinity of the sub-wavelength aperture, the secondary contribution from the surface plasmons launched and scattered on the exit surface narrows the divergence dramatically from that of a normal isotropic distribution. The coupling of the electromagnetic wave of the SP back to light follows the dispersion curve imposed by the periodic structure surrounding the aperture. In effect, the combination of the periodic corrugation momentum (G) and SP momentum (k_{sp}) on the exit side acts like a k-vector filter on the reradiated light (k_{out}) defining the permitted emission angle θ (i.e., $k_{out} \sin\theta = k_{out//} = k_{sp} \pm G$). As a result, in the linear symmetry of the slit configuration, off-axis beams can exist with wavelength-dependent angles. In the circular symmetry of the bull's eye structure, off-axis beams are forbidden by destructive interference; only beams normal to the surface can exist at a specific wavelength dictated by the corrugation period.

The micro-scaled metallic structures described here transmit light with a combination of low divergence, directionality and high efficiency. Their spectral and angular characteristics can be tailored over a wide range in a one-step lithographic process by corrugating the surface lateral to the propagation direction of the transmitted beam. Such devices can be thought of as miniature phased-array antennas in the optical regime, which can transmit or receive light along a specific direction for a given wavelength. Potential applications of these results include spatial and spectral multiplexing (i.e., rerouting of light according to wavelength), coupling in and out of fibers, and optimizing near-field devices for microscopy or data storage purposes. Furthermore, the diffraction-reducing properties of our structures might be applied to reducing the intrinsically high beam divergence of common optical devices such as light-emitting diodes (*21*) and semiconductor lasers (*22*). In summary, our findings show a unique path toward achieving photonic miniaturisation without the usual scaling limitations in the subwavelength regime, such as low transmittance and severe diffraction.

References and Notes

1. J. B. Pendry, *Science* **285**, 1687 (1999).
2. W. L. Barnes, *IEEE J. Lightwave Techn.* **17**, 2171 (1999).
3. S. C. Kitson, W. L. Barnes, J. R. Sambles, *Phys. Rev. Lett.* **77**, 2670 (1996).
4. J. R. Krenn *et al.*, *Phys. Rev. Lett.* **82**, 2590 (1999).
5. T. W. Ebbesen, H. J. Lezec, H. F. Ghaemi, T. Thio, P. A. Wolff, *Nature* **391**, 667 (1998).
6. H. F. Ghaemi, T. Thio, D. E. Grupp, T. W. Ebbesen, H. J. Lezec, *Phys. Rev. B* **58**, 6779 (1988).
7. D. E. Grupp, H. J. Lezec, T. Thio, T. W. Ebbesen, *Adv. Mater.* **11**, 860 (1999).
8. L. Martin-Moreno *et al.*, *Phys. Rev. Lett.* **86**, 1114 (2001).
9. A. Krishnan *et al.*, *Opt. Lett.* **200**, 1 (2001).
10. E. Popov, M. Neviere, S. Enoch, R. Reinisch, *Phys. Rev. B.* **62**, 16100 (2000).
11. J. A. Porto, F. J. Garcia-Vidal, J. B. Pendry, *Phys. Rev. Lett.* **83**, 2845 (1999).
12. L. Salomon, F. Grillot, A. V. Zayats, F. de Fornel, *Phys. Rev. Lett.* **86**, 1110 (2001).
13. S. Collin, F. Pardo, R. Teissier, J.-L. Pelouard, *Phys. Rev. B* **63**, 033107 (2001).
14. V. A. Shubin, A. K. Sarychev, J. P. Clerc, V. M. Shalaev, *Phys. Rev. B* **62**, 11230 (2000).
15. J. M. Vigoureux, *Opt. Commun.* **198**, 257 (2001).
16. P. T. Worthing, W. L. Barnes, *Appl. Phys. Lett.* **79**, 3035 (2001).
17. A. P. Hibbins, J. R. Sambles, C. R. Lawrence, *J. Appl. Phys.* **87**, 2677 (2001).
18. J. J. Greffet *et al.*, *Nature* **416**, 61 (2001).
19. E. Hecht, *Optics* (Addison-Wesley, Reading, MA, 1990).
20. A detailed theoretical analysis of the phenomena is beyond the scope of this report and will be presented in a forthcoming paper.
21. A. Köck, E. Gornik, M. Hauser, W. Beinstingl, *Appl. Phys. Lett.* **57**, 2327 (1990).
22. T. Erdogan *et al.*, *Appl. Phys. Lett.* **60**, 1921 (1992).

23. The near-field experiments were carried out in the Submicron Optics Laboratory of the University of Burgundy, and the authors are grateful for the assistance of Y. Lacroute, C. Chicanne, and A. Dereux. The assistance of Andreas Schertel (FEI Europe) as well as valuable discussions with T. Thio (NECI) are also gratefully acknowledged.

15 March 2002; accepted 28 May 2002
Published online 20 June 2002;
10.1126/science.1071895
Include this information when citing this paper.

Femtosecond Infrared Spectroscopy of Bacteriorhodopsin Chromophore Isomerization

Johannes Herbst, Karsten Heyne,* Rolf Diller†

The vibrational dynamics of the retinal chromophore all-trans–to–13-cis photoisomerization in bacteriorhodopsin has been studied with mid-infrared absorption spectroscopy at high time resolution (about 200 femtoseconds). After photoexcitation of light-adapted bacteriorhodopsin, the transient infrared absorption was probed in a broad spectral region, including vibrations with dominant C–C, C=C, and C=NH stretching mode amplitude. All photoproduct modes, especially those around 1190 reciprocal-centimeters that are indicative for a 13-cis configuration of the chromophore, rise with a time constant of ~0.5 picosecond. The results presented give direct vibrational-spectroscopic evidence for the isomerization taking place within 0.5 picosecond, as has been suggested by previous optical femtosecond time-resolved experiments but questioned recently by picosecond time-resolved vibrational spectroscopy experiments.

Bacteriorhodopsin (bR) is a light-driven proton pump that has served as a model system for the study of protein-based, ultrafast, light-induced trans-cis isomerizations. It represents an entire class of retinal-containing proteins with similar photochemistry but very different biological functions, such as visual transduction in rhodopsin, chloride pump in halorhodopsin, and photoreception in sensory rhodopsin (*1*). In all of these seven-helical transmembrane proteins, a retinal chromophore is covalently bound by a protonated Schiff base (SB) to a lysine (Lys) residue. Photons electronically excite the chromophore and drive a C=C double-bond isomerization, which in bR transforms the all-trans into the 13-cis configuration.

Photoisomerization initiates a series of